The performance of high resolution particle velocimetry : algorithm, simulations and experiments

The performance of high resolution particle velocimetry: algorithm, simulations and experiments

R.J.M. Bastiaans, G.A.J. van der Plas and R.N. Kieft

Eindhoven University of Technology,
P.O. Box 513,
NL-5600 MB Eindhoven, The Netherlands.

CIP-DATA LIBRARY TECHNISCHE UNIVERSITEIT EINDHOVEN

Bastiaans, R.J.M.; Plas, G.A.J. van der; Kieft, R.N.

The performance of high resolution particle velocimetry: algorithm, simulations and experiments / by R.J.M. Bastiaans, G.A.J. van der Plas and R.N. Kieft - Eindhoven: Technische Universiteit Eindhoven, 2001. - EUT Report 2001-W-001. - ISBN: 90-386-2792-0 NUGI 812
Subject headings: PTV / PIV / fluid dynamics / velocity measurement

Abstract

In this report we investigate the performance of particle tracking, exploring the influence of an increasing amount of estimators. Basically, a simple method to determine particle matchings was used. Then, first, temporal extrapolation as well as spatial interpolation are employed. Second, a PIV processing step was incorporated. Tests from simulations show that at relatively high seeding densities the performance was increased with a factor of 4 and 13 for the first and second step, respectively. In a physical experiment of a wake behind a heated cylinder a clear performance improvement in the case of PIV preprocessing was observed.

keywords: PTV, PIV, fluid dynamics, velocity measurement

Contents

1 Introduction

Flow visualisation and velocity estimation by means of using tracer particles is a very old and well-established technique. A very common way of investigating flow fields in this way is to illuminate tracer particles seeded in a fluid with a thin sheet of light. The images of the moving particles in the light sheet can be recorded and processed, see figure 1. With the application of photogrammetric devices, like photo-, film- and video-cameras, many high resolution images can be recorded. Therefore, large amounts of detailed quantitative information about velocities in fluids can be obtained.

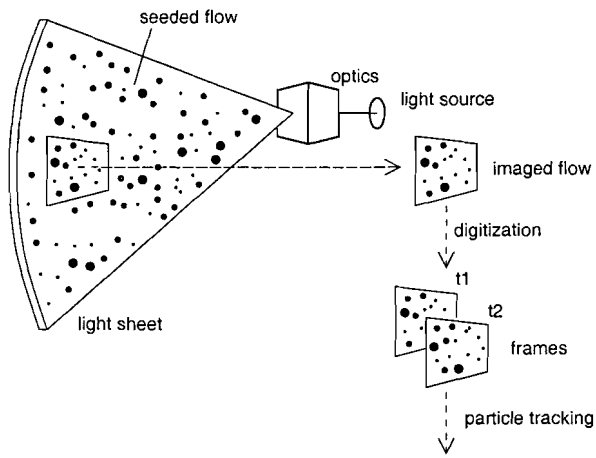

Figure 1: General experimental setup for particle tracking.

Currently several techniques, based on the above visualisation technique, have been developed to measure the 2D-velocity field in a flow. Each technique has its own method of image recording and processing to extract the velocity data. Several of these techniques, e.g. Particle Tracking Velocimetry (PTV) and Particle Image Velocimetry (PIV) are quite well known. In PTV individual particles are tracked in subsequent images whereas in PIV the averaged displacement of particles is determined in corresponding image segments of two sequential images. These methods can also be applied to one multiple exposed image.

Keane et al. [11] were one of the first to combine the techniques of PTV and PIV. They used the PIV estimation of the local convoluted velocity field as an input for the PTV processing. In the PTV step the displacements of all individual particles are reconstructed. This technique, which we will call High Resolution Particle Velocimetry (HRPV), has two significant advantages: both the accuracy and the resolution of the velocity estimation are increased. Resolution is increased because using PIV to estimate a particle's displacement allows a PTV algorithm to search a smaller region for a particle match. Thus seeding density can be increased. This is confirmed by results obtained by Keane et al. [11]. On the account of accuracy, Cowen and Monismith [6] show that PTV algorithms can inherently be more accurate than correlation-based PIV algorithms. One of the reasons for this is that the PTV is relatively unaffected by the presence of displacement gradients.

An additional advantage of HRPV is that the need of having several sequential images to achieve a successful particle tracking result at relatively high seeding densities is circumvented. In HRPV two images are sufficient to obtain tracking results. This is useful in situations where it is not possible to obtain more than two sequential images due to practical limits.

In this report we investigate the performance of both PTV and HRPV algorithms. Compared to the wide variety of existent PTV algorithms there is a large consensus about the PIV processing of image recordings. Therefore we take a standard cross-correlation PIV method, with proven performance, for the present HRPV processing. A large number of PTV methods are described in the literature (e.g. [7], [8], [9], [10], [12], [15], [16], [17], [18], [19], [24] and [28]). Many PTV-algorithms are quite complicated, computationally expensive and sensitive to its settings and the recorded flows. Therefore it was decided to develop a straightforward well defined PTV algorithm suitable for the present purpose, i.e. analysing the performance of PTV

and HRPV. Furthermore the new PTV method serves as a bases for the development of a three-dimensional PTV-code of which first results are reported in Kieft [13] and Schreel et al. [21]. First results of the present 2D PTV-code were already presented in van der Plas and Bastiaans [22].

The report starts with a description of the PTV-algorithm in section 2. Besides the application of a minmax-filter it differs essentially from other methods in the solver of the matching problem. This solver is developed on the basis of solution methods for the well-known assignment problem (e.g. Winston [27]). It turns out that a very simple, efficient and computationally cheap and straightforward method can be deduced. In section 3 the applied PIV is described after which the combination of PIV and PTV into HRPV is treated in section 4. The performance and operational parameters of the algorithm for PTV and HRPV are determined by tests with synthesised image data, which are given in section 5. In section 6 the algorithm was tested using experimental data of Kieft et al. [14] who investigated the flow phenomena occurring in the wake behind a heated cylinder. Due to the induced heat, stable vortex structures shed from the cylinder become disturbed. These heat induced disturbances grow, as the vortex structures are convected downstream, and manifest themselves as small mushroom type vortex structures. For tracing these mushroom type structures both accurate and detailed measurement of the flow field is necessary. The report ends with conclusions on the different methods in section 7.

2 The PTV algorithm

2.1 Components of the method

In figure 2 the flowchart of the separate parts in the PTV algorithm are shown. In this paragraph the functions of the individual components are summarised.

First the visualised images are dynamically thresholded to remove background intensity variations (dynamic thresholding). Thereafter the images are processed to obtain the pixel coordinates of the particles present in the images (blob detection). Next pixel coordinates are re-mapped from pixel coordinates to a physical coordinate set (mapping). Then, particles of a frame $f + 1$ are linked with particles from frame f by the matching algorithm. If a match is established between particle images of the different subsequent frames, these particle images are labelled to originate from the same physical particle which has moved a little in time.

Generally a particle image (or shortly "particle") with number i in frame $f+1$ is matched with the closest particle j in frame f. However particle j may already be occupied by another particle or may not be the best candidate in a global sense, i.e. if all other matchings are considered. Therefore a global optimisation must be carried out (matching). This matching can be improved by not using the real position of the particles in frame f but instead using an estimation of their position in frame $f + 1$. The estimation may originate from extrapolation in time as well as interpolation in space. The estimated position is provided by the prediction algorithm (prediction).

In case the predictor gives insufficient information, external information from file can be retrieved for each frame on demand (background velocity reader). For HRPV the external information are the results obtained by PIV. The next paragraphs explain the relevant modules of the tracking algorithm in more detail.

2.2 Dynamic thresholding

Particle detection is almost trivial since the particles appear as bright spots on a dark background. Sometimes the background intensity is non-uniform due to the reflections and the non-uniform intensity profile of a light sheet. Generally high-pass filtering is applied to remove background intensities. However this also changes the intensity profile of the particle image and thus influences the particle position that is calculated from it.

We preferred to perform a non-linear form of dynamical thresholding to remove the background. A simple and fast algorithm was chosen: a square min-max subtraction filter. The filter leaves the intensity profile undisturbed while removing non-uniformities with the size of the filter. The filter consists of three basic operations:

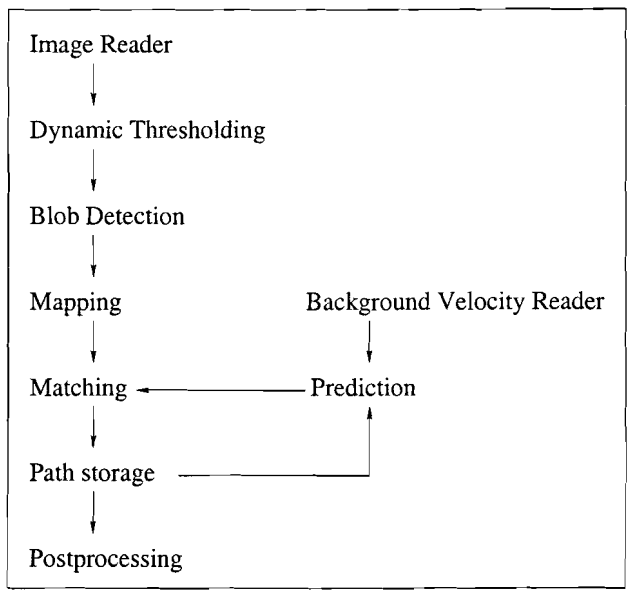

Figure 2: Overview scheme of the particle tracking algorithm.

Step 1: Min Each pixel in a copy from the original image is replaced by the minimum value in a square filter window.

Step 2: Max Each pixel in the Min filtered image is then replaced by the maximum value in the square filter window.

Step 3: Sub The result of step 2 is then subtracted from the original image.

Steps 1 to 3 of a one-dimensional min-max subtraction filter, performed on a one-dimensional function f(x), are shown in figure 3.

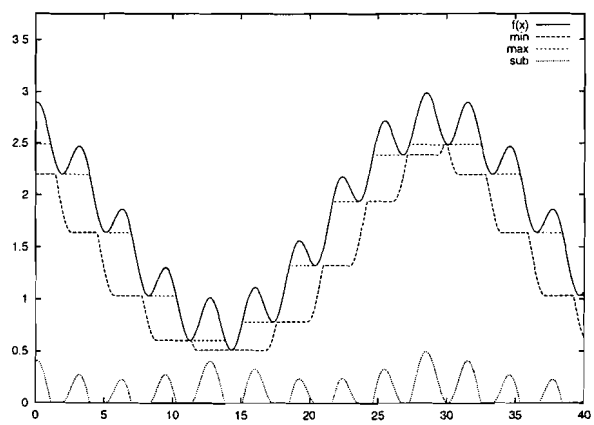

Figure 3: One-dimensional representation of the separate steps of the min-max subtraction filter (with width of 5).

A rectangular window was chosen, although a circular window is more suitable when dealing with circular shaped particle images. A rectangular window is separable. It can be obtained by a line filter in the x-direction followed by a line filter in the y direction. Line implementation in rectangular windows can be implemented in nearly size-independent processing time by using updating, see Verbeek et al. [23]. In contrast a circular window takes a processing time that is linear with the window size when implemented using

updating. The window width and height should correspond with the maximum width and height of particles one wishes to detect. The difference between circular and square windows are small in practice, since for small filter sizes (particle sized, i.e. typically 5x5 or smaller) the circular shape approaches the square window shape.

2.3 Blob detection

The algorithm for blob detection is rather simple. Pixels that have a vertical or horizontal neighbour are called connected to each other. Regions of connected pixels in an image with an intensity higher than a specified threshold level are called blobs. The single threshold is set slightly above the noise level. Since the images are dynamically thresholded a single threshold is sufficient. The detected blobs fulfilling certain shape and intensity criteria are then accepted to be valid particle images.

Only minimum required blob size and maximum allowed blob size are currently implemented for the validation. Furthermore, blobs that are connected to the edges of the image are not accepted as valid particles. This because these blobs may be part of much larger structures. Moreover, the centre of these blobs can not be determined, which is essential to PTV. Small particles as used for tracking will appear round with a Gaussian-like shaped intensity profile due to the characteristics of the imaging optics. In special cases where noise, reflections, and small background effects remain after dynamic thresholding one can easily add shape and intensity criteria as needed. Dalziel [7] for example, used additional criteria (e.g. maximum ellipticity, minimum required averaged intensity), to distinguish real particle images from particle sized intensity blobs.

After this validation step, the particle positions are determined with sub pixel accuracy by using the grey value weighted centre of gravity (volume centroid) of the segmented blob as in Dalziel [7] and Maas et al. [15]. Cowen and Monismith [6] performed Monte Carlo simulations with Gaussian shaped particles. Their results show that for 3 and 5 points estimates of the absolute position the volume centroid estimate is slightly less accurate than a Gaussian estimate.

2.4 Mapping

The positions of detected particle images are determined in pixel coordinates by the blob detection part and have to be translated back to physical positions in the light sheet. This translation between pixel coordinates and world coordinates is complicated due to the optical distortions from lenses and differences in the refractive indices of water, glass and air. Moreover, calculating the relations between particle position in the light sheet and the particle image in the frame from the position and composition of the separate elements in the experimental setup is quite laborious. Employing an in-situ calibration technique is a more practical solution.

Commonly, just before starting measurements, a known grid is placed inside the light sheet and an image of it is recorded. From this grid image the world and pixel coordinates of a set of N_r reference points can be determined. These reference points are then used to determine the M coefficients ($M \leq N_r$) of a mapping function for translating pixel coordinates to world coordinates.

In most cases there are no steep gradients in the image distortion and a global bilinear or biquadratic mapping function as implemented in our mapping module is sufficient. The equations for determining the coefficients are solved with least squares fitting using singular value decomposition.

2.5 Matching

For the matching procedure one may define an evaluation function to express the likelihood that one particle image in one frame and another particle image in the next frame corresponds to the same particle in the flow field. A solver using the evaluation function is then applied to find the best set of pairings between two images. The following basic evaluation function is used:

$$c_{ij}^{f} = \left| \mathbf{x}_i^{f+1} - \mathbf{x}_j'^{f} \right|, \tag{1}$$

where $\mathbf{x}_j'^f$ is the estimated position of particle j from frame f in frame $f+1$. If there is a good estimation of the movement of the particles or if the displacements are very small, then low values of c_{ij}^f correspond to a high probability that two particle images originate from the same physical particle.

Suppose that the average inter-frame displacement of particles is smaller than the mean minimum distance between particles. Then the majority of particles will be matched correctly even if no prediction scheme is employed, i.e. we have zero-order prediction. Higher orders of spatial and temporal prediction will be available after tracking several frames and this improves the matching results significantly. Earlier experiences with the algorithm of Dalziel [7] showed this to be true and this is confirmed by the results later on in this article.

There are several things an adequate solver should do. First the solver should find a set of independent matchings. A matching between particle i from frame f and particle image j from frame $f+1$ is denoted by $\alpha_{ij}^f = 1$, otherwise $\alpha_{ij}^f = 0$. A set of matchings is defined to be independent if

$$\forall i \sum_j \alpha_{ij}^f \leq 1 \quad \text{and} \quad \forall j \sum_i \alpha_{ij}^f \leq 1. \tag{2}$$

Furthermore the set should contain as much matches as possible. The maximum number of possible matchings is determined by the minimum number of observed particle images over the two fields involved. Finally, the sum of $\alpha_{ij}^f c_{ij}^f$ over all values of i and j should be as low as possible. The problem of finding the optimal set of relations between two data sets defined by an evaluation function is known as the assignment problem in operations research (see e.g. Winston [27]) and can be solved by the extended Munkres algorithm as developed by Bourgeois and Lassalle [5].

However, the Munkres algorithm has three disadvantages. First, it tries to match particles for evaluation function values representing distances larger than the maximum inter frame displacement of particles. Second, a large matrix of the evaluation function values has to be stored and third, solving requires much computation time, proportional to N_p^3, with N_p the number of particles found in a field.

The first disadvantage can easily be solved by defining a restriction on the maximum matching distance, $\Delta r_{\max}$, beyond which no valid relations can occur. The added restriction of a maximum matching distance allows a different, easier solution of the problem. A simple solver was developed which globally optimises for pairings up to a specified maximum matching distance. At the same time it uses a much smaller sized sparse matrix and it is considerably faster. This, so called 'sort matching' algorithm, works as follows:

step 1: Store all values of the evaluation function, c_{ij}^f, of possible pairings within the defined maximum matching distance, $\Delta r_{\max}$, in a sparse matrix.

step 2: Sort pairings on size of these evaluation function values.

step 3: Determine independent set of pairings, starting with the lowest value of the evaluation function. The lowest value corresponds to a match. Subsequent values correspond to matchings if both partners i and j of the pair are still unmatched, i.e. if $\sum_j \alpha_{ij}^f = 0$ and $\sum_i \alpha_{ij}^f = 0$.

For sorting a standard "Quicksort" routine is being used (see e.g. Press et al. [20]). The implementation of the matching algorithm as described above results in a computational processing time which is a fraction of the total PTV execution time.

2.6 Prediction

The tracking can be improved by using the estimated positions in the current frame of particles from a previous frame, instead of the real position of these particles. For this purpose two prediction algorithms are applied, a spatial and a temporal algorithm. Basically first a temporal extrapolation of the particle path is calculated to estimate the new position. If this is not possible, i.e. if there are no previous matchings, a spatial interpolation is calculated using surrounding matched particles. If the amount of information in a specified surrounding is not sufficient, then spatial interpolation of velocities from an external source, like PIV, can be invoked. The next two paragraphs describe the temporal and spatial scheme subsequently.

Scheme 1: Temporal extrapolation of the particle path

Although more sophisticated approaches are possible like those given in Pervez and Solomon [19] and Yagoh et al. [28], a simple algorithm can be satisfactory in most cases. For each particle i in image frame f extrapolation is calculated by Lagrange's extrapolating polynomial of degree $N_t - 1$ through the last N_t points of its path as given by

$$\mathbf{x}_i'^f = \sum_{k=1}^{k=N_t} A(k, N_t)\mathbf{x}_i^{f-k} \tag{3}$$

with

$$A(k, N_t) = (-1)^{k-1}\frac{N_t!}{k!(N_t - k)!}. \tag{4}$$

The maximum order of the polynomial can be specified. Tests with synthesised data have been performed in section 5 to determine the effect of higher order polynomials. Results show that, for the case considered, the performance of the tracking algorithm is highest for $N_t = 2$, although larger values of N_t result in a good performance as well. Application of $N_t = 1$, i.e. no temporal prediction, results in a clearly lower performance.

Scheme 2: Spatial interpolation

Spatial interpolation is performed using information of neighbouring matched particles or external velocity information, for example PIV-data. In case of neighbouring matched particles k, the estimated position is calculated by

$$\mathbf{x}_i'^f = \mathbf{x}_i^f + \frac{\sum_k \rho_k \left(\mathbf{x}_k^f - \mathbf{x}_k^{f-1}\right)}{\sum_k \rho_k}. \tag{5}$$

In case of external velocity information the estimated position is calculated in an analogous way by

$$\mathbf{x}_i'^f = \mathbf{x}_i^f + \frac{\sum_k \rho_k \cdot \mathbf{u}_k}{\sum_k \rho_k} \cdot \delta t, \tag{6}$$

with the weighting function ρ_k having a characteristic width Δ. Possible options for ρ_k are:

- Top-hat

$$\rho_k = \begin{cases} 1 & \text{if } \left|\mathbf{x}_i^f - \mathbf{x}_k^f\right| < \Delta; \\ 0 & \text{otherwise.} \end{cases} \tag{7}$$

- Gaussian

$$\rho_k = \exp\left(\frac{-\left(\mathbf{x}_i^f - \mathbf{x}_k^f\right)^2}{\Delta^2}\right). \tag{8}$$

Now ρ_k is a measure of the amount of information in a specified surrounding. If ρ_k exceeds a specified threshold, spatial interpolation is employed, invoking surrounding matched particles. Otherwise the presence of an external source, containing space and velocity information, is checked. In this case spatial interpolation on the basis of the external (PIV) data may be performed.

2.7 Post-processing

The stored particle path data can be used directly or used to calculate particle velocities. For comparison with our synthesised test images, the velocities of a particle at frame f were calculated from the positions from its particle track by a central second order scheme:

$$\mathbf{u}_p^f = \frac{\mathbf{x}_p^{f+1} - \mathbf{x}_p^{f-1}}{2\delta t}. \tag{9}$$

This scheme as well as a first order forward scheme and a fourth-order scheme were compared by Malik et al. [16]. For their data the second order scheme was reported to be the most accurate one by far.

3 The PIV algorithm

In order to perform the HRPV a PIV correlation technique is used to estimate the displacements of groups of particles. The employed PIV algorithm is based on standard 2D FFT's. These are applied to corresponding interrogation areas of the subsequent single exposed images. Therefore it is a cross-correlation method. The average displacement of the particles in an interrogation area is determined by the localisation of the centre of the correlation peak. An estimation of this position is obtained by a Gaussian fit according to Willert [26]. This is based on the assumption that particle images and therefore the covariance function are approximately Gaussian shaped.

Velocity gradients in an interrogation area are responsible for a gradually increasing loss of correlation at larger displacements. This is caused by the fact that particle pairs at high velocity have a larger chance of being advected over the borders of the interrogation area. Therefore as according to Westerweel [25] a correlation correction factor can be calculated. In order to deal with the in-plane particle loss this factor is applied in the present algorithm.

A measure for the quality of the correlation is given by the ratio of highest and second highest peak. The quality of the correlation can be used to discard unreliable data. A more detailed description of the PIV algorithm, together with accuracy tests, is given in Bastiaans [4].

4 High resolution particle velocimetry

Now the described PTV and PIV techniques can be combined to HRPV. Of course this can only be applied in a satisfactory way if the seeding density full-fills some requirements. For the PIV estimation the image density should be within upper and lower limits to obtain a well defined correlation. Furthermore the spatial velocity fluctuations within an interrogation area should be relatively small. Therefore there is a minimum amount of particles required to represent a flow structure adequately. Additional limits for the seeding density are given by the PTV processing step. A high seeding density would be preferable to obtain a high resolution velocity field sampling. However, in the PTV method the necessity to identify single particles is even more severe, when compared to PIV. The PIV identification of particles is performed by using a threshold. Thus it is important to have a minimum amount of overlapping particles. For randomly distributed particles the fractional amount of overlapping particle images, P_o, is given by Bastiaans [4] as

$$P_o = 1 - e^{-4N_s}, \tag{10}$$

in which N_s is the source density according to Adrian [1]

$$N_s = \frac{\pi}{4} d_e^2 \frac{C\Delta z_0}{M^2}, \tag{11}$$

for particles of image diameter d_e at concentration C. The thickness of the light sheet is Δz_0 and the magnification is denoted by M. Therefore at constant concentration the thickness of the light sheet is limited. Furthermore a large advantage of the HRPV procedure is the possibility to process sequences with a large displacement $\Delta s_{\max}$ compared to the mean distance between nearest neighbouring particles r_n. The number of particles per unite area is $C\Delta z_0$ and the mean distance between nearest neighbouring particles in the planar projection of the light sheet is then

$$r_n = (4C\Delta z_0)^{-1/2}. \tag{12}$$

The theory of the HRPV procedure was described and evaluated by Keane et al. [11]. In an experiment of analysing turbulent flow PIV data they found an increase of spatial resolution by a factor of 2.5 in each direction. Furthermore Cowen and Monismith [6] employed the technique with synthesised images and for images recorded from a turbulent boundary layer. They conclude that the results of the application of the HRPV method are superior to the results attained by PIV alone. This in the sense that not only resolution can be improved but also that the accuracy can be enlarged.

The difference of the present method with the two mentioned above is in the particle tracking algorithm. Both Keane et al. [11] and Cowen and Monismith [6] use a window method defining the estimated area to

which a particle advects. If there are two particles in this window the matching is ambiguous and must therefore be discarded. Obviously no matching can be established when there is no particle at all in this window. By minimising the global constraint, as specified in the matching algorithm section 2.5, the present PTV method should be able to obtain a larger yield without loss of accuracy.

Thus the advantages of using HRPV compared to PIV are the enlarged yield and accuracy. With respect to PTV the advantages are the ability to process only two sequential images at relatively large image densities and image sequences with relative large advection distances. This can be done with only a small maximum matching distance, $\Delta r_{\max}$, obtaining high quality data.

If we are not dealing with a starting flow, the PTV algorithm as described in previous sections shows a transient in the quality of the output. Errors could be kept low by using a small maximum matching distance, but then the yield will show a transient starting at very low values to higher values due to the neighbourhood estimation. However this will work only if the seeding density per flow structure is high enough, a condition that also has to be met for performing a successful PIV. Thus, if the seeding density per flow structure is large enough an additional advantage is obtained by the application of HRPV by omitting the transients.

The HRPV algorithm is implemented by considering the background displacements estimated by PIV as additional matchings in the neighbourhood estimation. By omitting the temporal extrapolation we obtain a separated scheme for PIV estimation and PTV matching. Involving also the temporal extrapolation results in a mixed scheme in which only the displacement of previously unmatched particles is estimated by both the surrounding matchings of PTV as well as the PIV displacements. Besides performing a PIV estimation for the entire sequence the implementation can handle the use of PIV estimation of one image pair for the entire sequence in case of steady flow or statistically steady turbulent flow (with relatively low turbulence intensity). Furthermore the present HRPV processing is also able to handle sequences in which there is only a random set of PIV estimations of all possible subsequent image pairs.

5 Performance tests with synthesised data

5.1 Synthesised image data

The developed algorithm was tested with synthetic images of a well defined flow field. The synthetic images were composed of several components representing important features of real image sequences. The images are grey level images with 256 grey values, 0 to 255. Particles are represented as Gaussian shaped intensity blobs. For each pixel value the particle intensity is integrated over the pixel area. An example of a test image is shown in figure 4. High wave number noise as well as background variations can be added easily.

The stream function describing the 2D vortical flow field chosen for advecting the randomly distributed particles is given by

$$\psi(x,y) = \sin(\pi x) \cdot \sin(\pi y) \tag{13}$$

on $\Omega = (0,1) \times (0,1)$. The velocity, $\mathbf{u}$, can be calculated with its definition,

$$\mathbf{u} = \left(\frac{\partial \psi}{\partial y}, -\frac{\partial \psi}{\partial x} \right). \tag{14}$$

Particle trajectories can be integrated using a series expansion with respect to time, up to any order. A 10th order expansion was implemented (more details are given in Bastiaans [4]). For the time steps that are used in the present study an accuracy of at least 10^{-6} image width per time step is guaranteed. For the image size of 512^2 this translates to $5 \cdot 10^{-4}$ pixel per time step. The flow is depicted in figure 5. The maximal particle displacement $\Delta s_{\max}$ occurring in the image is $\pi \delta t$. Because of the shear in the flow one is allowed to study the effects of merging and separation of particles on the performance of the tracking algorithm. The lack of particle loss across the boundary allows tracking for long periods without seeding new particles in the flow. Furthermore, the absence of singularities in the flow keeps the particles evenly distributed over the image.

5.2 Tracking and algorithm parameters

The performance of the tracking algorithm is influenced by the quality of the image sequence and the setting of the tracking parameters. The quality of the measured image sequence determines whether or not tracking

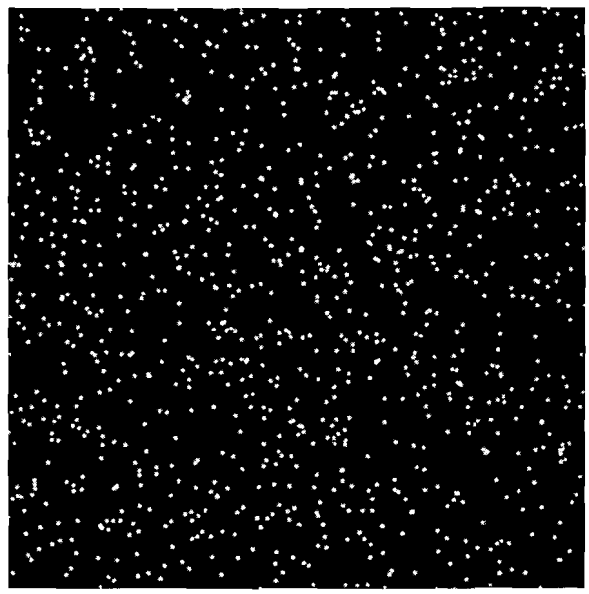

Figure 4: Test image of 512x512 pixels containing 1024 particles.

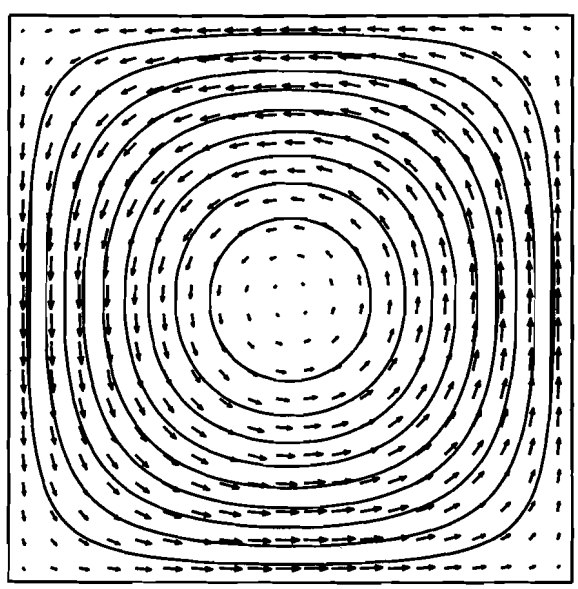

Figure 5: Velocity vectors and streamlines of the test flow.

results representative for the measured flow field can be obtained. The quality is determined by two important factors, the image quality (q_i) and sampling quality (q_s). A good image quality implies low noise and well detectable particle blobs in an image. The sampling quality means how well the particle tracks can be reconstructed. Therefore, both q_i and q_s depend on the source density N_s as defined in equation (11). However, for the synthetic image sequences in which distances are measured in pixels and the number of particles N_p is known, the source density can be rewritten as

$$N_s = \frac{\pi}{4} d_e^2 \frac{N_p}{A_I}. \tag{15}$$

Then the mean minimum particle distance is given by

$$r_n = \left(\frac{A_I}{4N_p} \right)^{\frac{1}{2}}, \tag{16}$$

with the particle diameter d_e and the image area A_I measured in pixels and square pixels, respectively. At high source densities individual particles can not be discerned from each other anymore and PTV processing will fail. Therefore we consider relatively low source densities.

For determining the sampling quality of an image sequence the displacement of the particles between images with respect to the mean minimum inter particle distance is of importance. If there is no information available about the displacement field, a high value of the maximum particle displacement, $\Delta s_{\max}$, compared to the mean minimum particle distance, r_n, results in a high uncertainty about which particle images correspond to each other. Therefore the sampling quality is expressed as the ratio between r_n and $\Delta s_{\max}$, occurring between two images,

$$q_s = \frac{r_n}{\Delta s_{\max}}. \tag{17}$$

This sampling quality gives an indication of the track-ability of an image sequence which can be understood by considering the effect of an increasing $\Delta s_{\max}$ for a constant r_n.

Besides the quality of the image sequence the algorithm parameters are also of importance for the tracking results. The choice of values for the maximum matching distance, the prediction order, and the neighbour weighting function width, Δ, is just as important as the image sequence quality.

5.3 PTV tests with synthesised images

Some tests were performed to determine the influence of image sequence quality and algorithm parameters on the performance of the particle tracking algorithm. An overview of the different tests and their parameter values are shown in table 1. From the tracking results the fractional yield (γ) and the mean velocity error ($\mu_{|\Delta v|}$) were determined per image and analysed. The overall performance, η_v, of the tracking is expressed as

$$\eta_v = \frac{\sqrt{\langle \gamma_v \rangle}}{\langle \mu_{|\Delta v|} \rangle}, \tag{18}$$

with time averaged quantities denoted by $\langle \cdot \rangle$ and the velocity yield, γ_v, is the number of particle paths with sufficient length to calculate the velocity using equation (9). For each test performed the above quantities were calculated and analysed. Each test consisted out of an image sequence of 100 images. Each image of 512^2 pixels contained 1024 particles. The half-width σ_p of the Gaussian shaped particles was set to $\sigma_p = 1.5$ pixels. This results in a source density of $N_s = 0.0276$ and a fractional overlap of $P_o = 0.1046$. Furthermore, the fraction of particles that can not be validated because they are connected to the image edges is 0.0117. Therefore the maximum yield possible is 88.4 %. The mean minimum particle distance r_n amounts 8 pixels. The tests were run on a Unix-PC, with a Pentium MMX processor at 200MHz, taking circa one minute to process one image sequence.

Results of the experiments are discussed in the next paragraphs. The values of γ, $\mu_{|\Delta v|}$ and η_v of test-runs A and E are given in figure 6 and 7. Results of test-runs B, C and D will be summarised only.

Test run	$d_N \cdot 512$	$\Delta s_{\max} \cdot 512$	$\Delta r_{\max} \cdot 512$	$\Delta \cdot 512$	N_t
A	8	4	2 16 0.5	0	1
B	8	4 12 2	4 12 2	0	1
C	8	8	8	0	1 5 1
D	8	8	0.8 8 0.8	0	2
E	8	8	0.8 8 0.8	8	2

Table 1: Test parameters: mean minimum inter particle distance, r_n, maximum particle displacement, $\Delta s_{\max}$, maximum matching distance, $\Delta r_{\max}$, interpolation radius, Δ, and the number of points for temporal extrapolation, N_t. Distances are multiplied by 512 to express their values in pixels. A set of three numbers indicates a sequence of values in which the first number corresponds to the first value, the second number to the end value and the third number is the step size.

In test-run A an image sequence is taken with a relative high sampling quality of 2.0. The performance of the algorithm, without any prediction schemes, was tested for different maximum matching distances. Results show that the performance peaks at $\Delta r_{\max}$ equals $\Delta s_{\max}$. A logical result since a maximum matching distance smaller than the maximum particle displacement will certainly result in unmatched particles which in fact should be matched. A maximum matching distance larger than the maximum particle displacement will allow for unnecessary erroneous matching relations. However, the increase in mean velocity error at larger maximum matching distances is limited due to the global optimisation in the matching procedure.

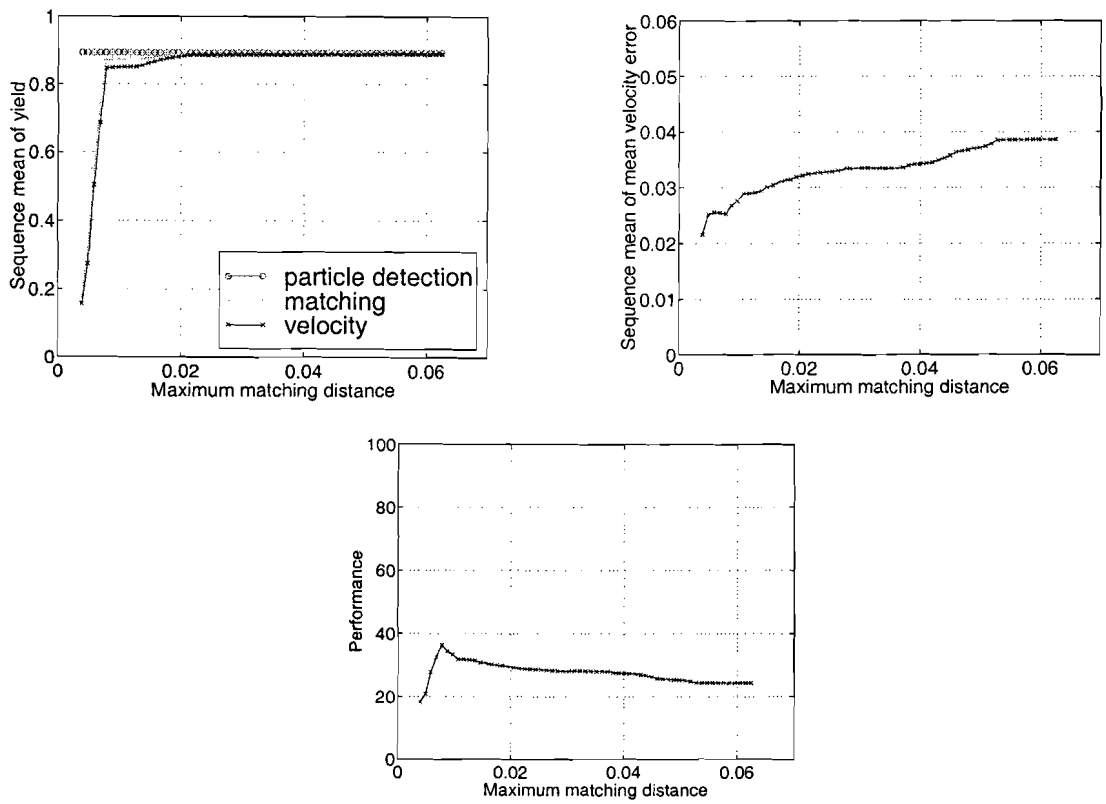

Figure 6: Results for test case A, $q_s = 2.0$.

The same algorithm settings were used in test-run B to test the influence of the sampling quality on the performance by varying the maximum particle displacement. The maximum particle displacement was varied with the sampling time for the images. The maximum matching distance was set equal to the maximum

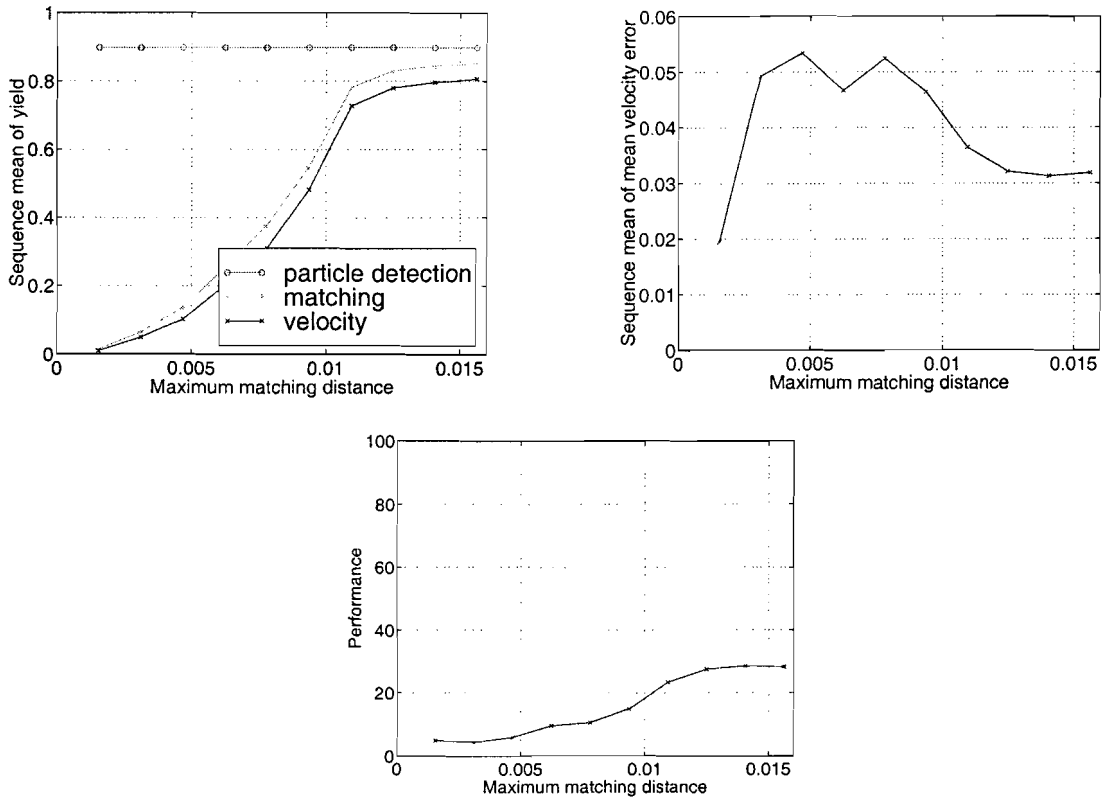

Figure 7: Results for test case E, $q_s = 1.0$.

particle displacement. This results in an increasing $\mu_{|Deltav|}$ and a decreasing γ giving a decreasing overall performance with a decreasing sample quality. At a sampling quality of $q_s = 2/3$ the performance is dropped from approximately 36 to about 2. A low sampling quality causes a large number of erroneous particles to be matched. As a result the average length of particle paths decreases, causing a decreasing value of the velocity yield.

The next tests are performed for a sampling quality of $q_s = 1$, which is a relatively difficult case for any PTV algorithm. Without a prediction scheme the performance is about 7, as obtained from test-run B. A sampling quality of 1 contains sufficient information to start tracking and there is ample room for improvement of the tracking result. In test-run C temporal prediction is used to improve the results. The success of the temporal prediction scheme depends of course on accuracy with which the particle position in the next frame can be expected. Flow dynamics, prediction scheme and magnitude of the error in the particle position are of importance. Clearly extrapolation order 1, $N_t = 2$, or higher is best, improving both the results for yield and accuracy. At these values the performance is increased from 7 to about 23. However, for order 4 extrapolation some decrease in the performance is observed. For this case the yield is still at a high level but the velocity errors start to grow. Since our test flow field only has large scales, the extrapolation errors are mainly caused by the the errors in the particle positions. These small errors may give poor estimations of the new particle positions at high orders of the temporal extrapolation.

Spatial prediction can be used to improve the matching yield of particles for which no temporal prediction is possible. This should improve yield an accuracy and, therefore, performance. Tests for comparing the results for tracking with and without spatial prediction were done with different maximum matching distance values in test-runs D and E. Again the sampling quality was 1 and N_t was equal to 2. In figure 7 results are shown for case E in which spatial prediction was activated. The results for D and E are similar in shape but the case which includes spatial prediction shows clearly an improvement in yield, accuracy and performance as expected. For the reference case the performance is increased from about 24 to about

28. Additional testing has shown that, for this type of large scale flow, the performance improvement due to spatial prediction is more or less constant for any reasonable value of Δ. Furthermore the sensitivity of the exact setting of $\Delta r_{\max}$ for the performance is decreased as can be observed from a comparison of test case A with E (figures 6 and 7). In test case A there is a sharp performance peak, whereas in test-case E the maximum is constant for a range of $\Delta r_{\max}$.

According to the above results, the best algorithm settings are $N_t = 2$, $\Delta r_{\max} = \Delta s_{\max}$ and Δ set to any reasonable value for the distances between particles. Of course also the scales in the flow must be taken into account. In the present case at $q_s = 1$ the mentioned settings of the algorithm result in an increase of the performance from 7, without any additional estimations, to 28, in the case of optimal settings. Sometimes the results can be improved somewhat by changing the parameters a little. One can easily think of certain situations where the presented optimal settings might not the best choice. For a stationary flow one could easily improve performance by decreasing the $\Delta r_{\max}$. Although at the first samples performance would be decreased, due to spatial prediction in the long run performance would improve. However in most cases the flow is dynamic and $\Delta r_{\max} = \Delta s_{\max}$ would be better.

5.4 HRPV tests with synthesised images

A further increase in performance is expected if the PTV algorithm is adapted for HRPV purposes. The spatial prediction code was extended in order to use the PIV results for the spatial velocity prediction. PIV was performed on frame 1 and 2 of the particular image sequence of test C, which has a sampling quality of 1. The size of the interrogation areas was chosen to obtain an image density of 16, i.e. the interrogation areas contain 16 particle images on average, in order to obtain a well-defined correlation. Thus, interrogation areas of 64 x 64 pixels are used, with an overlap of 32 pixels. This results in 15 x 15 interrogation areas of which there are only 8 x 8 independent data points. Therefore by using PIV alone the fractional velocity yield, γ_v, is only 1/16. The accuracy of the PIV estimation could be evaluated as well. However, the PIV results give an estimation of the convoluted velocity field, which is an estimation of the local velocity if the interrogation areas are small compared to the size of the flow structures. A comparison with actually obtained velocity vectors with the convoluted analytical flow field would fall beyond the scope of the present report. The PIV results were used for spatial prediction for processing the full sequence and they are shown in figure 8.

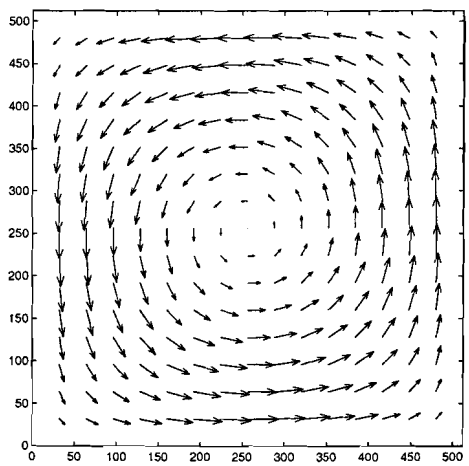

Figure 8: Obtained PIV velocity field as used for the HRPV processing.

The results of the HRPV are shown in figure 9. Clearly the HRPV result has a higher yield and accuracy and thus a much higher performance. The velocity yield is equal to the theoretical maximum yield, except for very small maximum matching distances. The mean velocity error stays constant at about 0.01 and the performance has a value of 92 to 98. Also one can see that the HRPV results are more or less independent of the maximum matching distance. At very small maximum matching distance the HRPV shows a slightly increased performance. Additionally, a smaller maximum matching distance allows for a smaller

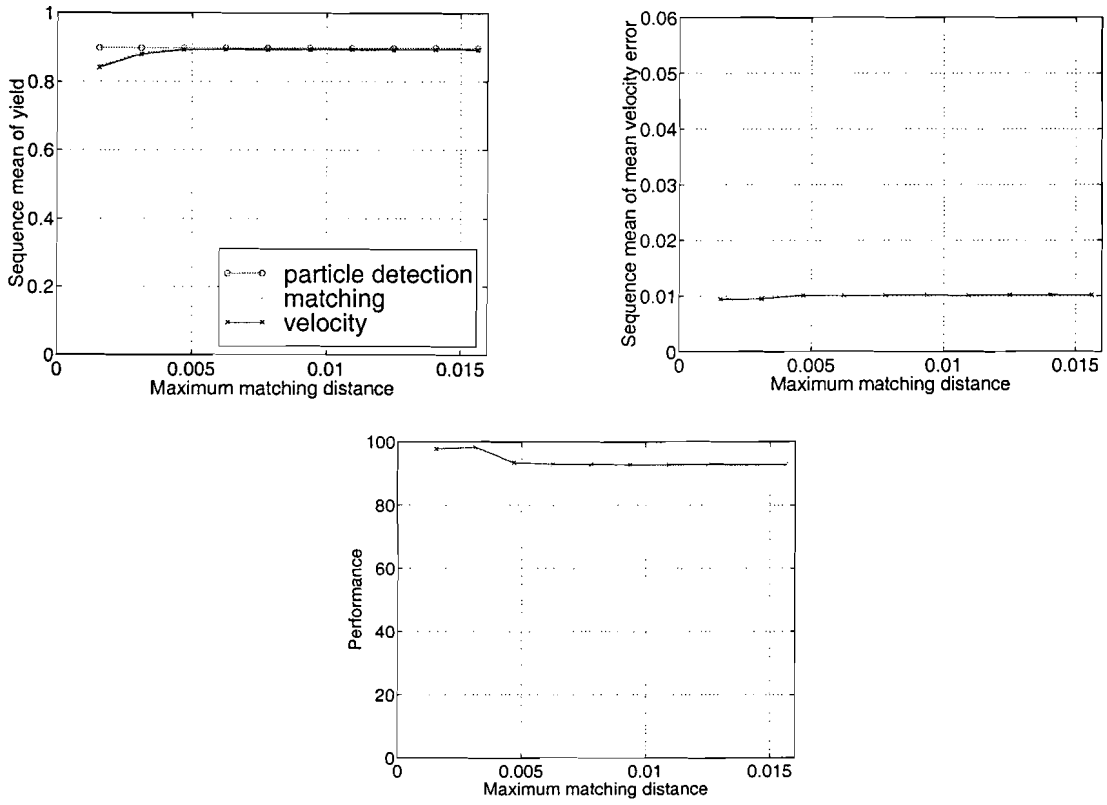

Figure 9: Results for the HRPV processing case, $q_s = 1.0$.

mean minimum particle distance, which can be used to increase the particle density and thus the resolution can be improved.

6 Tests with experimental data

6.1 Experimental setup

Since the synthesised images indicated that the algorithm performs in a satisfactory way, the next step is to test the algorithm with experimentally obtained data. The algorithm is tested on flow phenomena occurring in the wake behind a heated cylinder. The experimental conditions are schematically displayed in figure10.

For the experiments a water tank facility is designed in which the heated cylinder ($D = 8.5\,mm$, $L = 495\,mm$) is towed through the motionless tank rather then being exposed to a forced main flow. The specific dimensions of the water tank are for the $length \times width \times height = 500\,cm \times 50\,cm \times 75\,cm$. The main advantage of this device is a minimal creation of boundary layers and an almost uniform inflow velocity distribution (Anagnostopoulos [3]). To obtain the desired cylinder wall temperature an electric rod heater is used with a maximum heat density of $8.0\,W/cm^2$. The temperature of the cylinder is kept constant in time by controlling the heat input with the help of the measured wall temperature. The translation of the construction is obtained by an electric motor which is corrected for its variation in rotational speed by means of a closed circuit. This results in a variation in the rotational speed of less than 0.2 percent. The motor is coupled to the drive wheel by using a $1 : 100$ gear. Around the drive and the idle wheel of the translation system an almost inelastic fibre based tape is looped which is finally connected to the construction which carries the cylinder.

Hollow glass particles of size 10 and 20 μm are used as seeding. These particles are illuminated with a 200 mJ pulsed Nd:YAG laser. The recording is performed by using an eight bit digital camera with a

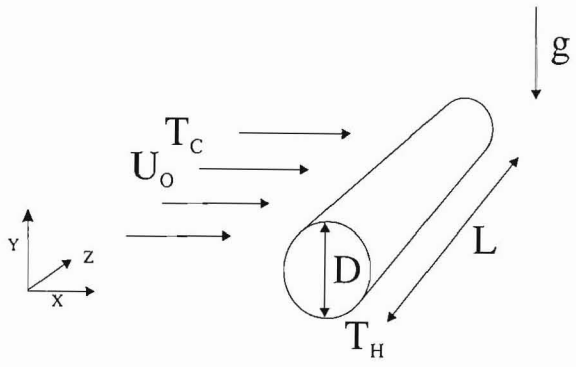

Figure 10: Definition of the mixed convection problem.

1008 × 1019 resolution at 29 Hz (Kodak ES1.0). The camera is directly coupled to the data acquisition system. The laser is synchronised by using the frame strobe of the camera as a master-signal. The method, as described above, resulted in an image sequence with relative low noise and well detectable particle images. An example of such an image is displayed in figure 11. More details about the experiment are given in Kieft [13].

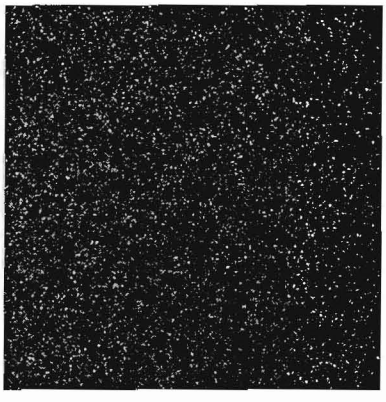

Figure 11: Typical image as obtained from the physical experiment.

6.2 Tracking and algorithm parameters

The blob detection and dynamical threshold parameters were optimised so that a maximum amount of particles could be detected. These parameters remained fixed during all tests. With this optimal set of parameters about 12,000 blobs were detected which results in a constant r_n equal to 4.6 camera pixels.

To get a good impression of the experimental performance of the algorithm it is sufficient to vary the sampling quality and measure the corresponding performance. This sampling quality can either be changed by varying r_n or Δs_{max}, according to equation (17). In the tests which are applied on the same sequence of acquired images, the image quality, q_s, is varied by skipping frames in the acquired image sequence. For a frame skip equal to 0, the subsequently grabbed camera frames are analysed while for a frame skip of k only the kth grabbed image is analysed. By doing so Δs_{max} (the displacement of particles between the analysed images) increases and therefore q_s decreases. In table 2 the applied frame skips are given together with the corresponding sampling qualities (equation (17)).

In the experimental case the exact solution of the flow field is not available. Therefore a more practical

skip	0	1	2	3	4	5	8	17
q_s	6	3	2	1.5	1.2	1	0.66	0.33

Table 2: Applied frame skips with corresponding sampling qualities q_s.

performance measure η_{ex} needed to be defined,

$$\eta_{ex} = \frac{\sqrt{(\gamma)}}{\sigma_{u,v}}, \tag{19}$$

where $\sigma_{u,v}$ denotes the mean standard deviation of the u and v component of the velocity vectors. This standard deviation is calculated by dividing the flow field into N_m monitoring areas in which the local standard deviation of the flow field is calculated with respect to the average velocity field within this small area. By averaging this local standard deviation over all monitoring areas $\sigma_{u,v}$ is calculated. For all tests, it turned out that $\sigma_u \approx \sigma_v$, therefore all further discussions are based on σ_u.

One should note that when N_m is taken too small (in other words the monitoring area is large), physical velocity gradients will contribute to the mean average standard deviation. On the other hand, by taking N_m too large, the amount of vectors on which the standard deviation in the interrogation area is evaluated becomes very small. In the presented results N_m is chosen to be 256 (16×16). As stated before, the physical velocity gradients will contribute to the local standard deviation. However, when there are no erroneous velocity vectors measured this standard deviation will be relatively low compared to the situation in which there are more and more erroneous velocity vectors. Therefore the local standard deviation is still a good qualitative measure of the errors. This holds analogously for the experimental performance.

In order to compare the performance of the PTV and HRPV method, the basis of these codes were chosen to be identical. This means that the blob detection, filtering and mapping are performed in a similar approach (figure 2). For the PTV code, no background reader was present, prediction was carried out using the information of the previous matching. For HRPV a prediction of the new particle location was obtained by using the background velocity fields which are obtained by running the PIV code on the same images as the ones used for the tracking.

6.3 Experimental results

For the tests as presented here, the HRPV results show a better performance than the PTV-results as can be observed in figure 12. For almost all chosen q_s, η_{ex} turns out to be higher for the HRPV results. Only for the largest q_s, this difference is small and even coincides for PTV and HRPV. However, for small q_s the difference is significant. Remarkable is the fact that the curve which represents the HRPV results does not show a maximum as can be seen in the PTV results, but increases linearly with decreasing q_s. The performance, presented here, is a combination of the total amount of velocity vectors found, expressed in the value of γ and the quality of these vectors which is expressed in the standard deviation of the vectors within a small sub domain ($\sigma_{u,v}$). In the figures 13 and 14 these separate quantities are presented. As one can see, for the PTV results, γ mainly increases as q_s decreases. This implies that for increasing frame skip more vectors can be found. This can be attributed to the fact that the accuracy of the sub-pixel interpolation becomes increasingly dominant. Therefore the errors in the temporal extrapolation increase rapidly. Then the present high seeding density results in lots of erroneous matchings. This can also be observed in the increase of the local standard deviation. The quality of the PTV vectors decreases rapidly for $q_s < 2$ (increasing σ_u). For the smallest q_s, this standard deviation is almost of the same order as the length of the velocity vectors.

For the HRPV results, the γ increases with an increase of sampling quality. However, the accuracy decreases more and therefore the performance shows a monotonic decrease. This behaviour can be understood by considering the particle location error, which becomes of minor importance for large particle displacements (small q_s).

Another approach to investigate the performance of the algorithms is by means of a vector field analysis. From the vector fields as depicted in figures 15 and 16, the higher performance of the HRPV algorithm can be seen by visual comparison. For $q_s = 6$, both vector fields (figures 15a and 16a) show no significant difference. The stray vectors which can be observed are mostly caused by the positional error in the particle

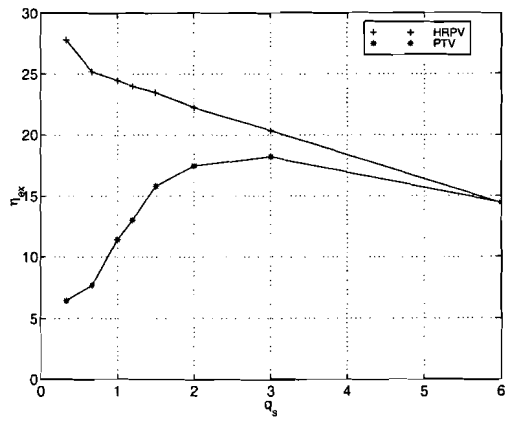

Figure 12: Performance for the PTV and HRPV tests as function of the image quality q_s based on the u component of the vector.

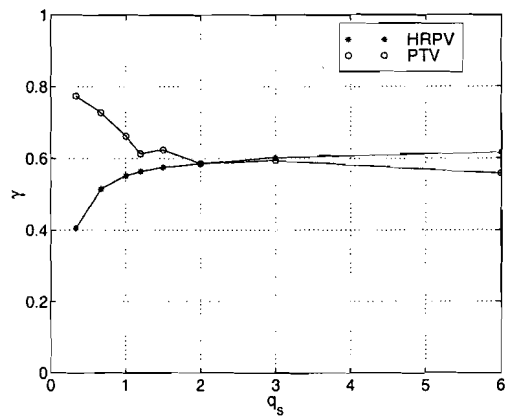

Figure 13: Velocity yield γ for the PTV and HRPV tests as function of the image quality q_s.

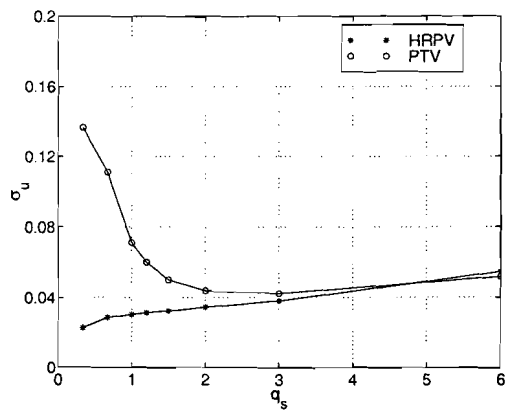

Figure 14: The σ_u for the PTV and HRPV tests as function of the image quality q_s.

location whose importance increases for increasing q_s (small displacements with respect to the inter particle distance).

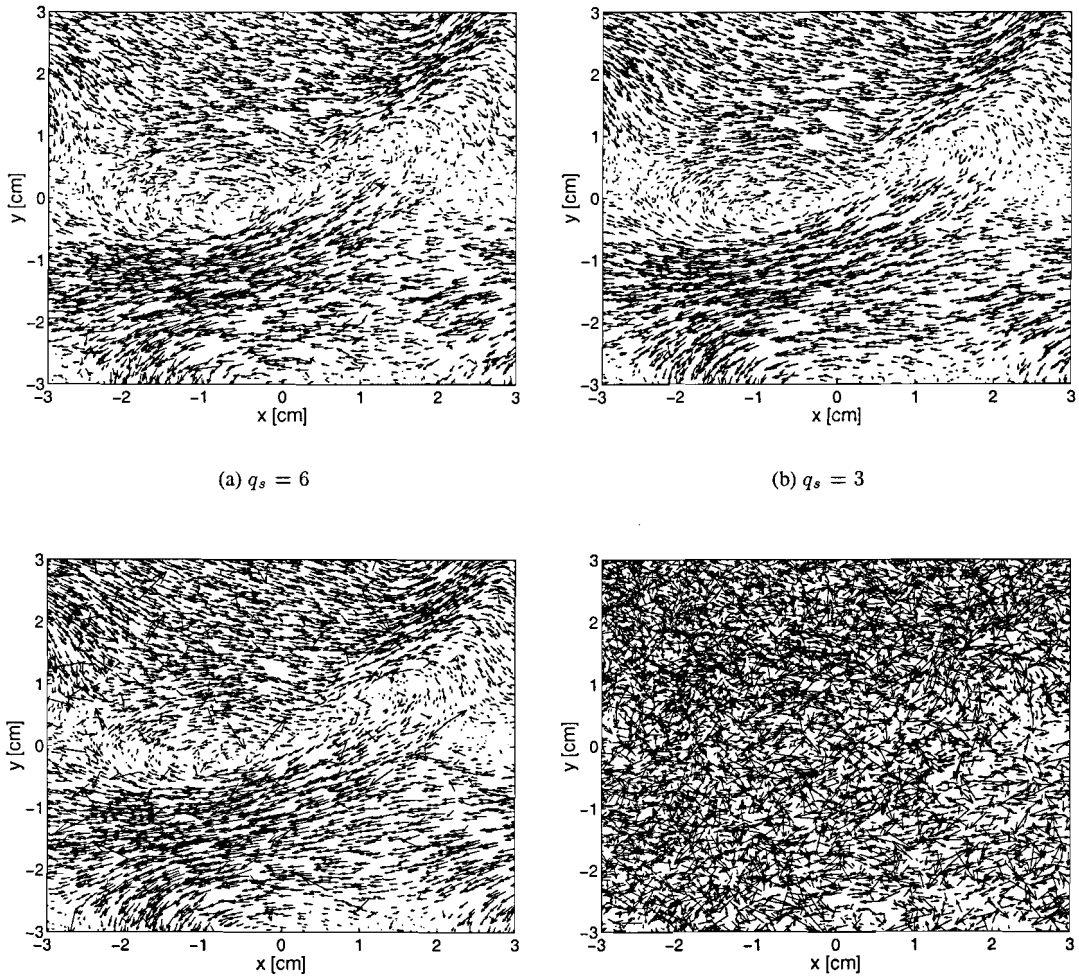

(a) $q_s = 6$

(b) $q_s = 3$

(c) $q_s = 1.2$

(d) $q_s = .333$

Figure 15: PTV vector fields at t=5 [s] for different sampling qualities.

As q_s decreases, first the quality of the vector field improves. The flow structures which can be found around $x, y = [-0.5,\ 0]$ and $x, y = [-0.5,\ -3]$ can be seen clearly as well as an escaping thermal structure at $x, y = [2,\ 2]$ (figures 15a,b and 16a,b). A further decreasing of q_s, results in a PTV-vector-field where more stray vectors can be observed, while for the HRPV vector field the quality remains constant or even improves (figures 15c and 16c). For the smallest q_s investigated, the PTV vector field appears as a random field of vectors, no coherent fluid flow can be detected. This means that no correlation can be found between particles in subsequent frames. The HRPV results on the other hand, still represents the flow field satisfactory. Only in the area where one finds large velocity gradients, some regions occur where less vectors are found. These regions were mainly caused by the low density of valid background velocity vectors. In the regions with large velocity gradients the PIV correlation between images was lost for large frame skips (small q_s). Therefore the invalid PIV estimated velocity vectors in these regions, as detected by the correlation peak height ratio, where discarded. The absence of a good velocity estimate for predicting particle positions results in a decay of the number of matches in the regions with large velocity gradients.

A more sensitive quantity to investigate the quality of the resulting vector field is the spanwise vorticity component ω_z, which is defined by

$$\omega_z = \frac{\partial v}{\partial x} - \frac{\partial u}{\partial y}. \tag{20}$$

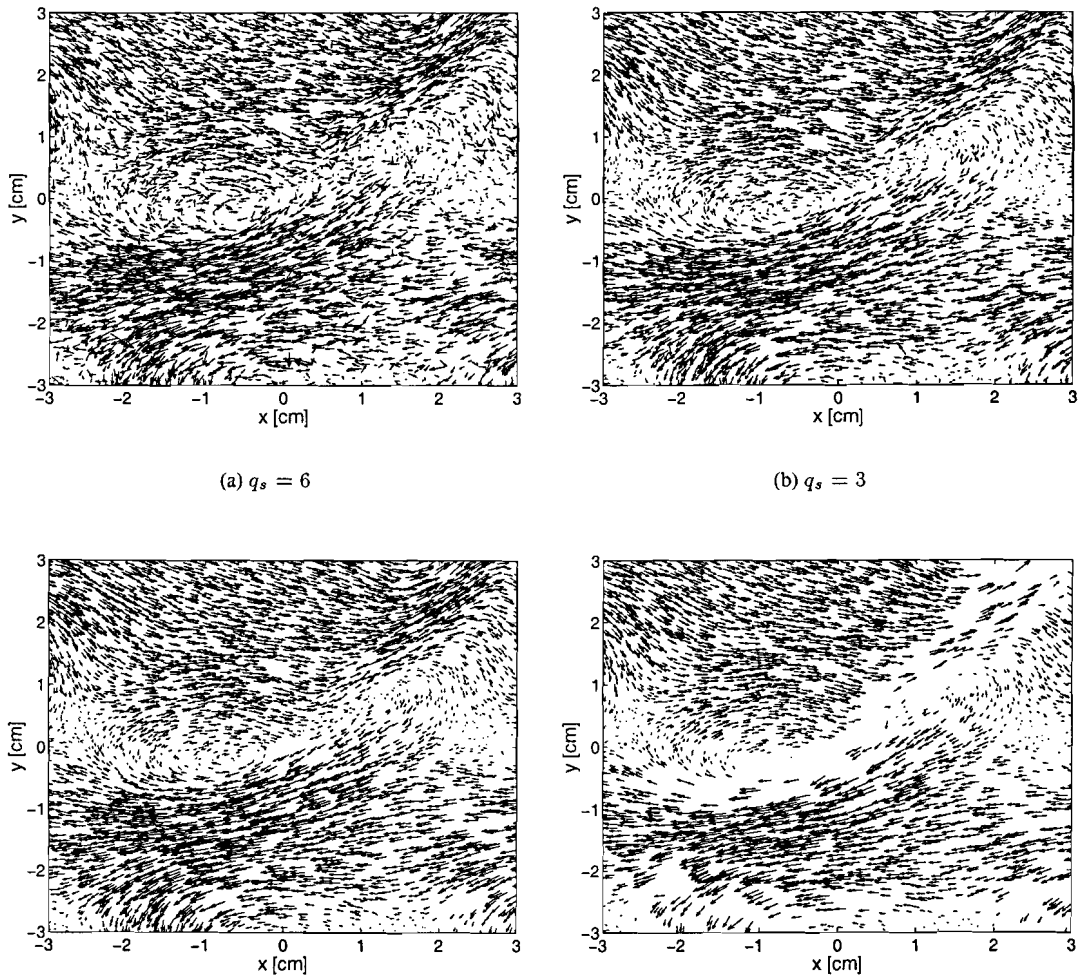

(a) $q_s = 6$

(b) $q_s = 3$

(c) $q_s = 1.2$

(d) $q_s = .333$

Figure 16: HRPV vector fields at t=5 [s] for different sampling qualities.

To calculate the vorticity, a Gaussian weighting method is used (Agui and Jimenez [2]) which interpolates the random distributed vector field on a regular grid on which the vorticity can be calculated by a central difference approach. By doing so, the vorticity is calculated from the presented vector field (Figs. 15 and 16). The PTV vorticity plots show that the best quality can be found for $q_s = 3$. Further decreasing of q_s results in a decrease of the quality eventually leading to a more or less chaotic vorticity distribution. For the HRPV results, the quality improves up to $q_s = 1.2$ and then decreases. The latter occurs due to the lack of information in regions of strong velocity gradient as already mentioned in the vector field discussion.

7 Conclusions

In the present report a particle tracking algorithm was introduced with a new straightforward matching procedure which turns out to be very efficient. It was used in combination with PIV to perform high resolution particle velocimetry. The algorithms were tested with synthetic and experimental data.

The tests with synthetic images show that the PTV algorithm is fast and accurate and for sampling quality values of 1 and larger a good overall performance value is achieved. The results also indicate that for optimal performance the algorithm parameter values should have the following values: $\Delta r_{\max} = \Delta s_{\max}$,

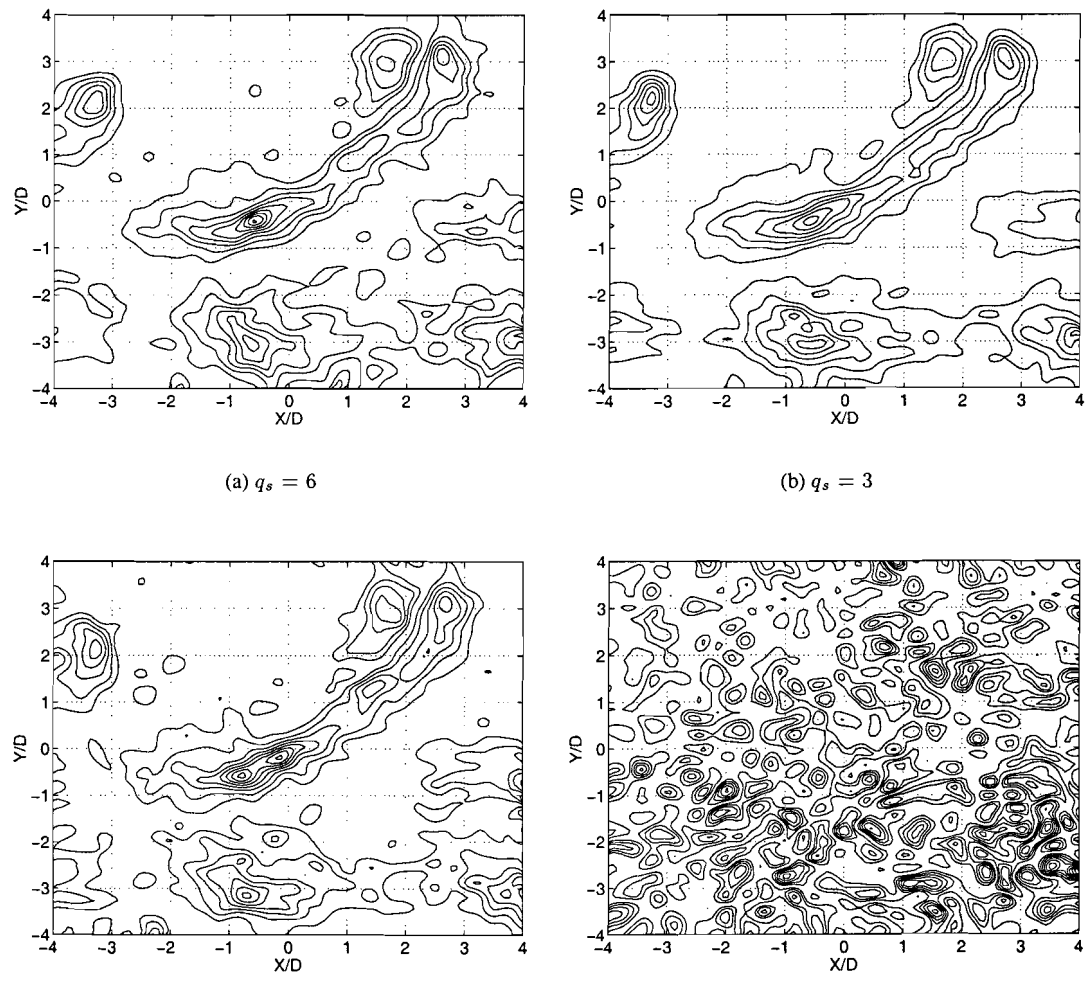

(a) $q_s = 6$ (b) $q_s = 3$

(c) $q_s = 1.2$ (d) $q_s = 0.33$

Figure 17: PTV vorticity distribution at t=5 [s] for different sampling qualities.

$\Delta s_{\max} < r_n$ (or $q_s > 1$), $N_t = 2$ and Δ at any reasonable value. In most cases $\Delta = r_n$ is reasonable if a Gaussian window is applied. It was shown that for a sequence quality of 1, which is quite difficult to track with high accuracy, the performance could be increased from about 7 to 28 by using nearby spatial and temporal information. In case of high resolution particle velocimetry, where a PIV estimation is used to enhance the results, a performance of approximately 98 is obtained and the sensitivity to the tracking parameters has become very low. Moreover, the highest resolution is determined by the lowest possible r_n, provided that the fractional overlap P_o is still small.

The experimental results presented here show that the performance of the HRPV algorithm turns out to be higher than that of the PTV algorithm, especially for image sequences where the particle displacements is larger than the mean minimum inter particle distance ($q_s < 1$). This corresponds largely with the results from tests with synthesised image sequences.

However, in the tests with the synthesised data the occurring error was dominated by erroneous matchings. In the experimental results this error is a combination of the erroneous matching and the particle position error. Especially for large values of q_s (very small displacements), the latter error turns out to be the most dominant one for both PTV and HRPV. For very small particle displacements this error can become of the same order as the length of the velocity vector. Here it should be noted that the crucial parameter is

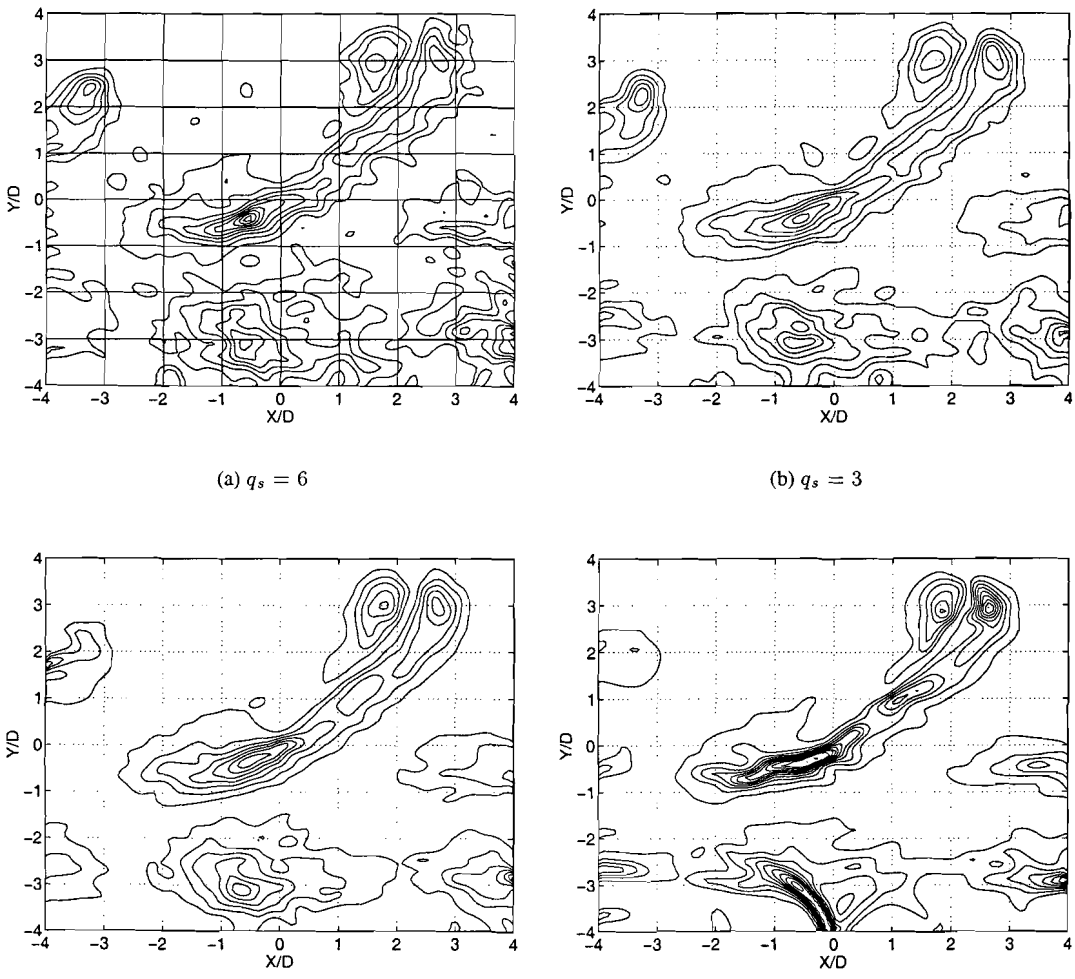

(a) $q_s = 6$

(b) $q_s = 3$

(c) $q_s = 1.2$

(d) $q_s = .333$

Figure 18: HRPV vorticity distribution at t=5 [s] for different sampling qualities.

then solely the particle displacement and not q_s.

For the HRPV results the accuracy of the obtained velocity vectors expressed in terms of a standard deviation of the vector field, remains high (small $\sigma_{u,v}$). This means that although the fractional velocity yield of the HRPV results decreases, the validity of the found vectors is more or less preserved. This in contrast to the PTV algorithm where the σ_u reaches a minimum at $q_s = 3$. For decreasing of q_s accuracy is lost fast due to random matching.

From the analyses of the vector and vorticity field it can be concluded that the HRPV algorithm performs optimally at $q_s \approx 1$. This difference in optimum performance with respect to the defined measure η_{ex}, occurs due to the fact that in this definition the accuracy is weighted stronger than the spatial resolution (expressed in γ). Furthermore, it turns out that the quality of the background velocity is of crucial importance to the performance of the HRPV algorithm. Missing vectors in this background velocity, due to ambiguous PIV correlations, cause a decrease of the velocity yield of the tracking results and therefore a decrease in performance. Thus in practice the possibility to generate adequate background velocity vectors determines the lowest limit of q_s for HRPV. In this particular case this limit can be found somewhere around $q_s \approx 0.5$.

An additional advantage of the HRPV algorithm is the possibility to obtain a qualitative good vector

field from just two images. This property makes it possible to perform particle tracking on two fast acquired images as obtained for example in measurements of high speed turbulent flows. The additional tracking then improves the spatial resolution strongly.

Acknowledgements

This research was funded by the Eindhoven University of Technology and the Dutch J.M. Burgers Centre for Fluid Dynamics.The experimental work here is part of the research programme of the Netherlands Foundation for Fundamental Research on Matter (FOM), which is financially supported by the Netherlands Organisation for Scientific Research (NWO). The authors would like to take the opportunity to thank the technical staff of the Energy Technology section for their support.

References

[1] R.J. Adrian. Particle-imaging techniques for experimental fluid mechanics. *Ann. Rev. Fluid Mech.*, 23:261–304, 1991.

[2] C. Agui and J. Jimenez. On the performance of particle tracking. *J. Fluid Mech.*, 185:447–468, 1987.

[3] E. Anagnostopoulos and J.H. Gerrard. A towing tank with minimal background motion. *J. Phys. E*, 9:951–954, 1978.

[4] R.J.M. Bastiaans. Cross-correlation piv; theory, implementation and accuracy. Technical Report EUT Report 99-W-001, ISBN: 90-386-2851-X, Eindhoven University of Technology, 2000.

[5] F. Bourgeois and J.C. Lassalle. An extension of the munkres algorithm for the assignment problem to rectangular matrices. *Comm. of the ACM*, 14(12):802–806, 1971.

[6] E.A. Cowen and S.G. Monismith. A hybrid digital particle tracking velocimetry technique. *Exp. in Fluids*, 22:199–211, 1997.

[7] S.B. Dalziel. Decay of rotating turbulence: some particle tracking experiments. In FTM Nieuwstadt, editor, *Flow Visualization and Image Analysis*, pages 27–54. Kluwer, 1993.

[8] T. Dracos and N.A. Malik. 3d particle tracking velocimetry - its possibilities and limitations. In *Proc. 6th Int. Symp. on Flow Visualization*, pages 785–791. Springer Verlag, 1992.

[9] Y.G. Guezennec, R.S. Brodkey, N. Trigui, and J.C. Kent. Algorithms for fully automated three-dimensional particle tracking velocimetry. *Exp. in Fluids*, 17:209–219, 1994.

[10] Y.A. Hassan and R.E. Canaan. Full-field bubbly flow velocity measurements using a multiframe particle tracking technique. *Exp. in Fluids*, 12:49–60, 1991.

[11] R.D. Keane, R.J. Adrian, and Y. Zhang. Super-resolution particle imaging velocimetry. *Meas. Sci. Technol.*, 6, 1995.

[12] B. Khalighi and Y.H. Lee. Particle tracking velocimetry: an automated processing algorithm. *Applied Optics*, 28(20):4328–4332, 1989.

[13] R.N. Kieft. *Mixed convection behind a heated cylinder.* PhD thesis, TUE, Eindhoven, The Netherlands, 2000.

[14] R.N. Kieft, C.C.M. Rindt, and A.A. Steenhoven. The wake behaviour behind a heated horizontal cylinder. *Exp. Thermal and Fluid Science*, 19(4):183–193, 1999.

[15] H.G. Maas, A. Gruen, and D. Papantoniou. Particle tracking velocimetry in three-dimensional flows, part 1. photogrammetric determination of particle coordinates. *Exp. in Fluids*, 15:133–146, 1993.

[16] N.A. Malik, T. Dracos, and D. Papantoniou. Particle tracking velocimetry in three-dimensional flows. Part II: Particle tracking. *Exp. in Fluids*, 15:279–294, 1993.

[17] K. Nishino, N. Kasagi, and M. Hirata. Three-dimensional particle tracking velocimetry based on automated digital image processing. *ASME Trans. J. Fluids Eng.*, 111:384–391, 1989.

[18] K. Okamoto, Y.A. Hassan, and W.D. Schmidl. New tracking algorithm for particle image velocimetry. *Exp. in Fluids*, 19:342–347, 1995.

[19] M.S. Pervez and T.H. Solomon. Long-term tracking of neutrally buoyant tracer particles in two-dimensional fluid flows. *Exp. in Fluids*, 17:135–140, 1994.

[20] W.H. Press, S.A. Teukolsky, W.T. Vetterling, and B.P. Flannery. *Numerical recipes in C, the art of scientific computing*, chapter 2.6. Cambridge Univerisity Press, 2nd edition, 1994.

[21] K.R.A.M. Schreel, G.A.J. van der Plas, and R.N. Kieft. Accuracy of a 3D particle tracking velocimetry method. In *Proceedings of the 9th International Symposium on Flow Visualisation*, Edinburgh 2000. CD-rom, paper 310, ISBN 0-9533991-1-7.

[22] G.A.J. van der Plas and R.J.M. Bastiaans. Accuracy and resolution of a fast PTV-algorithm suitable for HiRes-PV. In *Proceedings of the 8th International Symposium on Flow Visualisation*, Sorrento 1998. CD-rom, paper 87, ISBN 0-9533991-0-9.

[23] P.W. Verbeek, H.A. Vrooman, and L.J. van Vliet. Low-level image processing by max-min filters. *Signal Processing*, 15:249–258, 1988.

[24] M.P. Wernet. Fuzzy logic particle tracking velocimetry. In *SPIE Proceedings*, volume 2005, pages 701–708, 1993.

[25] J. Westerweel. *Digital Particle Image Velocimetry - Theory and Application* -. PhD thesis, Delft Univ. of Techn., The Netherlands, 1993.

[26] C.E. Willert. High resolution correlation peak detection. Technical Report ECE 251 C, UCSD, La Jolla, 1989.

[27] W. Winston. *Operations Research, Applications and Algorithms*, chapter 7. Duxbury Press, 1991.

[28] K. Yagoh, K. Ogawara, and S. Iida. The particle tracking method using the kalman filter. In F.T.M. Nieuwstadt, editor, *Flow Visualization and Image Analysis*, pages 838–842. Kluwer, 1993.